Central North Pacific SST Anomalies Linked Late Winter Haze to Arctic Sea Ice

Running Head: Pacific SST Linked Late Winter Haze to Arctic Sea Ice

Quan Yang [1], Dongmin Yuan [1,*]

[1]Key Laboratory of Meteorological Disaster, Ministry of Education/Joint International

Research Laboratory of Climate and Environment Change (ILCEC)/Collaborative

Innovation Center on Forecast and Evaluation of Meteorological Disasters

(CIC-FEMD), Nanjing University of Information Science & Technology, Nanjing

210044, China

*Corresponding authors: Dongmin Yuan

Address: No. 219 Ningliu Road, Pukou District, Nanjing University of Information

Science & Technology, Nanjing 210044, China

Email: dongmin_yuan@163.com (DY)

Telephone: +86 13655161661(DY)

Abstract

Haze pollution in the North China Plain is becoming more serious and consequently causes inconvenience in daily life and harms health. The interannual variation of haze days in the North China Plain in late winter (February and March) is closely related to the East Siberian Sea and Chukchi Sea ice in October, and the Pacific sea surface temperature (SST) plays a key role in delivering the effects of the sea ice on the haze. When the East Siberian Sea and Chukchi Sea ice increases in October, the October and November SST in the region over Minami-Tori Shima and Midway Atoll decreases. This reduced SST then lowers the January and February SST around the northwestern side of the Hawaiian Islands. The lower SST around the northwestern side of the Hawaiian Islands modulates the atmospheric circulation and makes the diffusion conditions and water vapor conditions in the North China Plain more conducive to the accumulation and growth of pollutants. Large ensemble simulations from the Community Earth System Model validate the process whereby the East Siberian Sea

and Chukchi Sea ice affects the SST in the aforementioned regions. The effect of changes in the SST around the northwestern side of the Hawaiian Islands on the meteorological conditions over the North China Plain was verified by numerical experiments using version 4 of the Community Atmosphere Model.

1. Introduction

Haze has become a detrimental type of weather that reduces visibility and causes traffic problems and inconvenience in people's lives. More seriously, particulate matter contained in haze can enter the lungs and remain there for a long time, thereby posing a serious threat to the respiratory system and affecting human health (Kunii et al. 2002). From the visibility data from 681 meteorological stations, Zhang et al. (2012) concluded that the regions with high incidences of haze in China include the North China Plain, the Yangtze River Delta, the Pearl River Delta, and the Sichuan Basin. Among them, the haze in the North China Plain is not only frequent but also increasingly severe (Che et al. 2009; Quan et al. 2011), and severe winter haze pollution in the North China Plain now has a great impact on people's normal lives. Problems such as the formation mechanisms and contribution levels of various sources of regional haze pollution have

attracted attention (Ding and Liu 2014; Mu and Zhang 2014; Wang et al. 2014b; Zhang et al. 2014).

Previous studies have shown that increased aerosol emissions and topographic conditions are important in causing intense haze pollution to form (Mu and Zhang 2014; Wang 2018; Wang et al. 2014a; Yang et al. 2016; Zhang et al. 2014), while climate factors and meteorological conditions are important in causing haze pollution to change (Cai et al. 2017; Chen et al. 2019a; Ding and Liu 2014; Jacob and Winnerb 2009; Jia et al. 2018; Wang 2018; Yang et al. 2016;Yin et al. 2015; Yin et al. 2017; Zhang et al. 2016). At present, pollutant concentrations in North China are running at high levels (Wang et al. 2013), and meteorological conditions play an important role in the formation of haze pollution in North China (Yin and Wang 2017a; Yin et al. 2017). For example, the weakened East Asian winter monsoon inhibits the horizontal diffusion of pollutants and is conducive to the generation of haze (Li et al. 2016; Niu et al. 2010; Wang and Chen 2016; Yin et al. 2017), anticyclonic anomalies in the middle troposphere weaken the vertical diffusion of pollutants (Chen and Wang 2015; Yin and Wang 2017a; Zhong et al. 2019), increased water vapor increases the amount of moisture absorbed by pollutants and aggravates haze pollution (Chen and Wang 2015; Ding and Liu 2014), and reduced local precipitation reduces the wet deposition of pollutants, which is conducive to haze occurring (Wang and Chen 2016).

Large-scale circulation and meteorological conditions are affected by many external forcing factors, such as snow cover (Li and Wang 2014; Sun 2017; Xu et al. 2018; Yin and Wang 2018), sea surface temperature (SST) (Gao and Li 2015; Li et al. 2017; Li et al. 2008; Xiao et al. 2015; Yin and Wang 2016), and Arctic sea ice (Alexander et al. 2004; Lin and Li 2018; Mori et al. 2014; Wang and Liu 2016; Yin et al. 2019c). Among those factors, changes in the autumn sea ice impact the East Asian winter monsoon (Li and Wang 2013; Li and Wang 2014), the winter temperatures in China (Zuo et al. 2016), and the snowfall in northern and central China (Liu et al. 2012). Wang et al. (2015) found that decreased Arctic sea ice aggravates haze pollution in eastern China. However, Yin and Wang (2017b) succeeded in predicting changes in the number of winter haze days in the North China Plain using the Arctic sea ice and SST, and the increase of Beaufort Sea ice increased the number of winter haze days in North China. As another important external forcing factor, SST anomalies can affect atmospheric circulation, which in turn affects haze over China (Chen et al. 2019b; Wang et al. 2019; Yin and Wang 2016).

The impacts of changes in Arctic sea ice on haze pollution events are complex: changes in different regions of Arctic sea ice have different impacts on haze pollution events (Wang et al. 2015; Yin and Wang 2017b). Therefore, the detailed effects and mechanisms require further research. SST can also affect haze pollution in China. The

relationship between SST and Arctic sea ice and their influence on haze formation needs to be further studied. Herein, we discuss the influence and mechanism of sea ice in a specific region on haze pollution over the North China Plain. Previous studies have usually taken the haze days in winter (December, January, and February) as a whole to explore their relationship with external forcing and meteorological conditions. Chen and Wang (2015) showed that the frequency of haze occurrence is highest in December and January while that in February and March is second highest. Here, we focus on how Arctic sea ice affects the haze pollution in late winter (February and March) in the North China plain. In section 2, we introduce our data and methods. In section 3, we analyze the observational connections between Arctic sea ice and haze pollution. In section 4, the mechanisms whereby Arctic sea ice affects haze and the role of Pacific SST are analyzed. Finally, we present our conclusions and discussion in section 5.

2. Data and methods

The data for monthly geopotential height, wind, temperature, sea-level pressure (SLP), omega, specific humidity, and other meteorological conditions from 1979 to 2017 come from the National Centers for Environmental Prediction (NCEP) and the National Center for Atmospheric Research (NCAR). The data for monthly SST and sea-ice concentration (SIC) come from the Hadley Centre's sea ice and SST dataset

(HadISST1) (Rayner et al. 2003). The data for boundary-layer height (BLH) come from the Monthly Means of Daily Means data of the ERA-Interim dataset.

Haze is a multidisciplinary problem. In the field of environmental pollution, haze pollution is usually characterized by the concentration of PM2.5. However, the observation of PM2.5 started late in China, and the data is too short to meet the requirements of climate research. In the field of meteorology, haze is usually represented by visibility and humidity. Herein, we adopt the reconstructed haze-day data in late winter from 1979 to 2017 (Yin and Wang 2016; Yin et al. 2017). After strict quality control, the four-times-per-day meteorological observation data provided by the National Meteorological Information Center of China are used to reconstruct the haze-day data. The key meteorological elements used are wind speed, visibility, relative humidity, and precipitation. Firstly, other phenomena affecting visibility, such as precipitation, sandstorms and dust, are excluded. When the visibility is lower than a certain threshold and the relative humidity is less than 90%, haze is considered to occur. As long as this phenomenon occurs in one of the four observations, this day will be recorded as a haze day. More details about the reconstruction process are given by Yin and Wang (2016) and Yin et al. (2017). The accuracy of the reconstructed data has been verified in the two articles. By analyzing hourly visibility and atmospheric composition, it was found that the reconstructed haze-day datasets not only met the meteorological

standards, but also well represented the concentration of atmospheric components. Herein, we use the haze-day data from 34 stations in the North China Plain (NCP: 35°N–42°N, 114°E–120°E). The haze-day index (HDI) is calculated as the mean number of haze days in late winter in the NCP. To eliminate the influence of other factors such as economic development, all linear trends have been removed from the haze and meteorological data.

In this study, the Community Earth System Model Large Ensemble (CESM_LE) datasets and the simulations using version 4 of the Community Atmosphere Model (CAM4) are used to verify the relationship between Arctic sea ice, Pacific SST and haze pollution. All CESM_LE simulations use the same fully-coupled global climate model, namely, the Community Earth System Model, and the same radiative forcing scenario (historical up to 2005 and RCP8.5 thereafter) but begin from slightly different initial atmospheric states (Kay et al. 2015). Herein, we use 35 members of CESM_LE completed at NCAR containing the 20th century portion (1920–2005) and the RCP8.5 portion (2006–2100). The variables used here include SST, meridional and zonal winds, and sea-ice fraction. CAM4 is a global atmosphere model developed primarily at the National Center for Atmospheric Research. The results of sensitivity experiments with CAM4 are used to verify our proposed mechanisms. CAM4 adopts finite-volume dynamical core due to its superior transport properties (Neale et al. 2010). All

simulations use a latitude-longitude grid at the horizontal resolution of 0.9°×1.25° with 26 vertical hybrid sigma-pressure levels. CAM4 forced by climatological monthly mean SST and SIC data on a 1.0°×1.0° grid from the Hadley Centre. The coupling software calculates air-sea fluxes and maps them to the atmosphere model grid conservatively. The monthly outputs from CAM4 for wind, BLH, omega, and relative humidity are used for analysis.

3. Observational connections between Arctic sea ice and haze

The monthly differences in haze days in the NCP are considerable. Fig. S1(a) shows the interannual variation in the haze days in the four winter months in the NCP. The number of haze days was declining slowly before 2010 but then increased dramatically after 2010. The number of haze days in January and February has been changing at a considerably higher rate than those in February and March. It is worth noting that the number of haze days in late winter began to decline after 2013, whereas the number of haze days in December and January continued to increase. Fig. S1(b) shows the climatic mean numbers of haze days from December to March in the NCP. According to this figure, there are considerably more haze days in December and January than in February and March. Therefore, the combined number of haze days in February and March in the NCP is taken as a whole (i.e., that for late winter) and is selected as the

research object herein.

Fig. S2 shows the anomalies in atmospheric circulation and local meteorological conditions related to the haze in late winter in the NCP. At the height of 200 hPa, prominent easterly anomalies occur around 30°N over East Asia (Fig. S2(a)), weakening the East Asian jet stream. In the middle layer of the troposphere, the atmospheric circulation is similar to the eastern-Atlantic/western-Russia pattern (Fig. S2(a)). Here, the atmospheric circulation in late winter differs from that in previous studies (Yin and Wang 2017a; Yin et al. 2017) in that the negative height anomaly north of the Balkhash is not obvious and there is a prominent negative height anomaly over the Pacific Ocean. These differences in atmospheric circulation may be why the number of haze days in late winter differs from that in early winter. Over the NCP, there are upward-motion anomalies near the surface (Fig. S2(b)), causing the surrounding pollutants to accumulate in the NCP. The depressed boundary layer is not conducive to the vertical diffusion of pollutants (Fig. S2(b)). At the same time, the NCP is located to the southwest of the high-altitude anticyclonic anomalies, and the enhanced southeasterly wind anomalies weaken the horizontal wind speed in the middle and low troposphere (Fig. S2 (d)). The rising humidity is conducive to the hygroscopic growth of pollutants and the aggravation of haze pollution (Fig. S2(c)).

Wang et al. (2015) found that less pre-autumn Arctic sea ice can lead to more

winter haze days in eastern China. Yin et al. (2017) also found that the eastern-Atlantic/western-Russia pattern in winter, especially the anomalous high over the NCP, is closely related to the pre-autumn sea-ice pattern. As an important external forcing, does the pre-autumn sea-ice change also affect the atmospheric circulation characteristics over the NCP on haze days in late winter? Fig. 1(a) shows the correlation coefficient (CC) between the HDI in late winter and the Arctic SIC in October. It can be seen that the SIC in October in the region from the eastern part of the Laptev Sea through the East Siberian Sea to the Chukchi Sea (73°N–79°N, 131°E–155°W) is significantly positively correlated with the HDI. We use the average sea-ice concentration of this region as the sea-ice index over the East Siberian Sea and Chukchi Sea (hereinafter referred to as SI_SC) in October. There is no significant correlation between the HDI in the NCP and the SI_SC from November to January (Fig. S3). Fig. 1(b) shows the interannual changes of SI_SC and HDI from 1979 to 2017. For comparative convenience, the data are standardized. The changes in SI_SC and HDI have similar characteristics: before 2000, both SI_SC and HDI were reasonably constant; from 2000 to 2010, they both exhibited downward trends and then increased considerably; since 2014, they have both been decreasing. The CC between SI_SC in October and HDI in late winter is as high as 0.52 (0.44 before de-trending), exceeding the 99% confidence level. Analyzing the correlation between SI_SC and HDI suggests

that increased SI_SC in October leads to more haze days in late winter in the NCP.

4. The role of SST in Pacific and physical mechanisms

The mechanism whereby the October SI_SC affects the number of haze days in late winter in the NCP is interesting and worth researching. The change in SST is closely related to the change in SIC. Balmaseda et al. (2010) found that the impact of sea ice on the atmospheric circulation over the Euro-Atlantic sector depends strongly on the SST. SST is also an important external forcing factor affecting meteorological conditions over China. Atlantic Ocean SST anomalies influence the winter haze in China at interannual and decadal time scales (Xiao et al. 2015). Yin and Wang (2016) found the preceding autumn Pacific SST can impact the winter haze over North-Central North China Plain. In Fig. S2 (a), the prominent negative height anomaly over the Pacific Ocean may affect the positive height anomaly over the NCP, so we focus on the role of Pacific SST in the process whereby SI_SC affects the number of haze days in the NCP. Fig. 2 shows SI_SC and HDI are both related to the Pacific SST in October and November. From the CC between SI_SC and Pacific SST, the increase of SI_SC increases the local surface albedo and decreases the absorption of solar radiation, and the SST in the Arctic area decreases considerably. At the same time, the increased SI_SC causes a triple pattern in the SST anomalies in the Pacific. The SST increases

considerably around the Aleutian Islands and near the equator but decreases over Minami-Tori Shima and Midway Atoll (23°N–37°N, 150°E–170°W). The decreased SST region is significantly correlated with SI_SC, with most areas exceeding the 95% confidence level. Fig. 2 (b) shows the CC between HDI in the NCP and the October and November SST in the Pacific Ocean. The triple pattern is now more obvious. Overall, the reduction in SST over Minami-Tori Shima and Midway Atoll is significantly correlated with both HDI in the NCP and SI_SC. Thus, the SST over this region may be an important link between SI_SC and the number of haze days in the NCP. We adopt the negative average SST over this region as the SST index over Minami-Tori Shima and Midway Atoll (SST_MM) in October and November, and its CCs with SI_SC and HDI are 0.43 and 0.42, respectively, both of which are significant at the 99% confidence level.

Increased sea ice induces cyclonic anomalies near the Aleutian basin and the Hawaiian Islands and anticyclonic anomalies near the Gulf of Alaska and the northwestern Pacific basin (Fig. 3 (a)). Affected by the anticyclone over the northwest Pacific basin and the cyclones over the Hawaiian Islands, prominent easterly anomalies appear in the western part of the area over Minami-Tori Shima and Midway Atoll, and northeasterly winds appear in the eastern part. These anomalies are present in the winds at both the lower troposphere and the surface (Fig. 3 (a) and (b)). The easterly anomaly

in the western part of the area over Minami-Tori Shima and Midway Atoll overlaps with the climatic easterly over this region, thereby accelerating the wind speed at the sea surface and reduces the SST by increasing evaporation in this area (Fig. 3(b)). In the eastern part of the area over Minami-Tori Shima and Midway Atoll, the abnormal northeasterly wind brings in cold sea water from high latitudes, thereby decreasing the SST of this area. The meridional wind index is calculated as the negative average meridional wind in this region in October and November. Fig. 3(c) shows the relationship between SST_MM and the meridional wind index in this region in October and November. It can be seen that the SST_MM is significantly positively correlated with the meridional wind index, the CC between them being as high as 0.62 and exceeding the 99% confidence level. That is, a northerly surface wind decreases the SST in this region.

The SST_MM in October and November affects the SST in January and February. The correlation between SST_MM and the Pacific SST in January and February is shown in Fig. 4(a). Clearly, the SST around the northwestern side of the Hawaiian Islands (20°N–37°N, 178°W–160°W) in January and February is strongly affected by the SST_MM: when the SST_MM decreases, so does the SST in that region. Furthermore, there is a close relationship between the HDI in the NCP in late winter and the SST around the northwestern side of the Hawaiian Islands in January and February

(Fig. 4(b)); this negative correlation indicates that when the SST there decreases, the HDI increases. The SST index of the northwestern side of the Hawaiian Islands (SST_NH) is calculated as the negative average January and February SST in this region (20°N–37°N, 178°W–160°W). The CC between SST_NH and SST_MM is 0.71, which is significant at the 99% confidence level. The CC between SST_NH and HDI in the NCP is 0.36, exceeding the 95% confidence level. Thus, by prolonging the abnormally low SST, the SST_NH is another important factor in influencing the number of haze days.

The processes whereby SST_MM in October and November affects SST_NH in January and February is shown in Fig. S4 and Fig. 5. Lower SST_MM trigger strong cyclonic anomalies in the northeastern Pacific basin in October and November (Fig. S4 (a) (c)). The initial baroclinic response of the atmospheric circulation to the SST forcing reaches its maximum amplitude in one week. After the initial baroclinic adjustment stage, the response gradually becomes more barotropic, and the spatial range and amplitude increase. This process takes about 2-2.5 months (Deser et al. 2007). In January and February, the barotropic structure of atmospheric circulation is more obvious and the spatial extent is wider (Fig. S4 (b) (d) and Fig. 5 (a)). The region over the northwest of the Hawaiian Islands dominated with strong northwesterly wind in response to those cyclones. This wind anomaly increases the wind speed at the sea

surface (Fig. 5(b)), and the increased wind speed accelerates evaporation and releases more heat, thereby reducing the SST in this area. The northwesterly wind also brings colder water from high latitudes, thereby further reducing the SST around the northwestern side of the Hawaiian Islands. The relationship between SST_NH and the wind field in January and February (Fig. 5(c)) shows that decreased SST_NH indeed has an important relationship with the northwestern wind anomaly.

We analyze the CESM_LE datasets to verify the effect of SI_SC on Pacific SST. For consistency with previous data, we choose the monthly outputs of CESM_LE from 1979 to 2017, with the data for 1979–2005 coming from historical simulations and those for 2006–2017 coming from the RCP8.5 scenario. We select the five years with the highest SI_SC in October and the five years with the lowest for each ensemble member of experiments (135 years in total) and analyze the SST and wind-field data from October to November of the corresponding years to reveal the relationship between SI_SC and SST_MM. However, according to the SI_SC only, the selected areas of increased sea ice are farther south and closer to land edges than were the areas analyzed previously, which would lead to biased results. To reduce the deviation caused by sea-ice in the south region, the sea-ice data have been screened to exclude those involving large SIC near land edges. Fig. S5 shows the deleted sea-ice data, in which the center of the sea ice anomaly is to the south of the land edges. The composite

differences for the retained sea-ice data are shown in Fig. 6(a), and the results for the SST and the wind field are shown in Fig. 6(b) and (c), respectively. As SI_SC increases, affected by the anticyclone of the northwest Pacific basin and the cyclones of the Hawaiian Islands, prominent easterly anomalies appear in the western part of the area over Minami-Tori Shima and Midway Atoll, and northeasterly winds appear in the eastern part, which favors lower SST_MM in October and November. These results agree well with previous observational results.

In a similar way, we use the SST and wind-field data from January to February in the corresponding low- and high-SST_MM years to reveal the relationship between SST_MM in October and November and SST_NH in January and February. The differences in the wind field show a strong cyclone in the northeastern Pacific basin, and the differences in SST show a considerable decline around the northwestern side of the Hawaiian Islands (Fig. 6(d) and (e)). The CESM_LE results further verify that the SST plays a crucial role in delivering the effects of SI_SC anomalies on the number of haze days in the NCP.

From Fig. 4(b), SST_NH in January and February and HDI in late winter are significantly correlated. SST_NH can affect haze pollution in the NCP by changing the atmospheric circulation and meteorological conditions in late winter (Fig. 7). Decreased SST_NH causes prominent negative pressure anomalies over the Pacific region and

positive ones over northeast Asia from 500 hPa to 200 hPa (Fig. 7(a)). At 200 hPa, there are prominent easterly anomalies at 30°N over Asia that weaken the East Asian jet stream. The negative pressure anomalies over the Pacific Ocean and the positive pressure anomalies over northern China in mid-tropospheric layer are very similar to the atmospheric circulation related to late winter haze analyzed in Fig. S2. At the same time, there is an upward movement at the surface in the NCP, and the BLH decreases (Fig. 7(b)). Consequently, the surrounding pollutants concentrate in the NCP and the vertical diffusion weakens, thereby aggravating the pollution in the NCP. When the SST_NH decreases, considerably enhanced southeasterly wind anomalies appear in the middle and lower troposphere (Fig. 7(a) and (d)), allowing humid air from the ocean to enter the NCP. This rising humidity is conducive to increased hygroscopic growth of pollutants, which degrades the environment (Fig. 7(c)). Meanwhile, with the pressure gradient weakened and the southeasterly wind anomaly increased, the horizontal wind speed over the NCP is reduced considerably (Fig. 7(d)), which leads to weakened horizontal diffusion of pollutants. These factors are conducive to the formation of haze, which means that decreasing SST_NH in January and February helps increase HDI in late winter.

We use CAM4 to verify the impact of SST_NH in January and February on the number of haze days in the NCP in late winter. This model runs for 50 years, and the

data of the last 30 years are taken as the control experiment. In the control experiment, the climatological monthly mean SST and SIC data from the Hadley Centre are used as the boundary conditions. In the sensitivity experiments, the SST anomalies around the northwestern side of the Hawaiian Islands from January to February in 2008 (high SST, hereinafter referred to as SEN_H) and in 2014 (low SST, hereinafter referred to as SEN_L) are superimposed on the SST field in the control experiment. During 1979–2017, 2014 saw the most haze days and 2011 saw the fewest, with 2008 seeing the second fewest (Fig. 1(b)). However, the difference in SST between 2014 and 2008 is larger than that between 2014 and 2011 (Fig. S6 (a)); thus, we choose anomalies superimposed on the SST field in 2008 and in 2014 as the boundary conditions in the sensitivity experiments. Fig. S6 (b) shows the differences in SST between two sensitivity experiments (2014 minus 2008). The ensemble of each sensitivity experiment contains 30 members. The 30-year data from the control experiment are used as the initial field of the sensitivity experiments. The initial conditions and boundary conditions of the two sensitive experiments were identical, except for the SST.

The differences in meteorological conditions in February and March between the results in SEN_H and SEN_L (SEN_L minus SEN_H), which represents the response of meteorological conditions in the NCP to decreased SST_NH, are shown in Fig. 8. When the SST_NH decreases, a strong cyclone is triggered over the Pacific Ocean and an

anticyclone is triggered near the Korean peninsula (Fig. 8(a)). At the same time, the BLH and wind speed at 10 m decreased (Fig. 8(b) and (c)). The dotted regions in Fig. 8(b) and (c) are where the changes from more than half of the 30 members in BLH and 10-m wind speed are consistent with the ensemble mean when SST_NH decreases. When SST decreases, an upward movement occurs at 925 hPa (Fig. 8(b)), which is conducive to the convergence and accumulation of pollutants. The relative humidity at 850 hPa increases, which is conducive to the hygroscopic growth of pollutant particles. Overall, the CAM4 results show that when SST_NH decreases, the vertical and horizontal diffusion conditions and humidity conditions in the NCP promote the formation of haze.

5. Conclusions and discussion

In this study, the meteorological conditions related to the haze in late winter in the NCP are analyzed. The results show that there is an intimate relationship between SI_SC in October and the number of haze days in the NCP in late winter, and the SST of the Pacific Ocean plays a crucial role in that relationship. When SI_SC increases in October, a high-pressure anomaly prevails over the northwestern Pacific basin and a low-pressure anomaly appears near the Hawaiian Islands. Under the influence of the consequent easterly and northeasterly winds, SST_MM decreases, which triggers a below-normal pressure anomaly in the basin of the northeast Pacific Ocean in January

and February. Under the influence of the northwesterly wind, SST_NH decreased. The physical process whereby SI_SC affects the SST in the Pacific has been verified by analyzing the CESM_LE dataset. Lower SST_NH in January and February triggers a strong cyclonic anomaly in the Pacific and abnormal high pressure around the Korean peninsula. The East Asian jet stream at 200 hPa and the East Asian deep trough at 500 hPa both weaken. In the lower troposphere, the BLH and the wind speed both decrease and the water vapor increases. These conditions are conducive to haze occurring and cause frequent haze pollution. The results of the CAM4 experiments driven by different SST also showed the effect of SST_NH change on the number of haze days in the NCP in late winter. Generally speaking, when SI_SC increases in October, SST_MM in October and November and SST_NH in January and February both decrease. Through air–sea interaction, the meteorological conditions over the NCP are affected, and the number of haze days increases. This process is shown schematically in Fig. 9.

Some studies have indicated that the northerly wind in the Arctic benefits an increase in the sea ice concentration (Deser and Teng, 2008). In the previous analysis in this article, the relationship between SI_SC and SST in October and November is analyzed, and the October and November atmospheric circulation is used as an intermediate to explain this process. In order to analyze whether the northerly wind

affecting the sea ice concentration also caused the SST decrease, we analyzed the relationship between the meridional wind index in October and the October and November atmospheric circulation and SST (Fig. S7). The meridional wind index was calculated as the negative average meridional wind in East Siberian Sea to the Chukchi Sea (73°N–79°N, 131°E–155°W) in October. The northerly wind that caused the increase of sea ice in October stimulated anticyclonic anomalies in the Aleutian Islands region in October and cyclonic anomalies in the region over Minami-Tori Shima and Midway Atoll. The circulations are different from the circulations caused by the increase of sea ice (the Fig. 3). In November, the CC between meridional wind index in October and circulation in the region over Minami-Tori Shima and Midway Atoll failed the reliability test. Therefore, the anomaly northerly wind that caused the increase of sea ice does not directly cause the decrease of SST, which also can be seen in the Fig. S7 (c). To verify the effect of sea ice change on circulation, experiments with the CAM4 are conducted. In this experiment, model also runs for 50 years, and the data of the last 30 years are taken as the control experiment. In the sensitivity experiment, we superimposed the sea ice anomalies over the East Siberian Sea and Chukchi Sea ice of October in 2007 (SIC_L) and in 2013 (SIC_H) to the sea ice in the climatic state. The forcing conditions and the initial conditions are identical except for the October sea ice over the East Siberian Sea and Chukchi Sea. The differences between SIC_H and SIC_L

output in October and November are used to see the change of circulation. As shown in the Fig. S8, changing sea ice triggers cyclone anomalies in the Aleutian and Hawaiian islands, and anticyclone anomalies in the Gulf of Alaska and the northwest Pacific basin. This is consistent with the results obtained by reanalysis data. Obvious easterly anomalies appear in the region over Minami-Tori Shima and Midway Atoll, and northerly wind occurs in the western part of this area, which is similar to the previous analysis. The CAM4 experiment shows that changing sea ice can affect atmospheric circulation.

As is known to all, SST is closely related to El Niño- Southern Oscillation (ENSO), so whether ENSO plays a role in the process of sea ice affecting haze? In the Fig. S9, we selected Niño3.4 index (https://www.esrl.noaa.gov/psd/data/correlation/nina34.data) to analyze the correlation between ENSO and haze in later winter. It can be seen that from October to February, ENSO has little influence on the haze in late winter in NCP. Although ENSO has a linkage effect with SST, we believe that ENSO is not directly involved in the process of sea ice affecting haze.

According to Fig. S1, winter is divided into early winter and late winter, and the number of haze days in late winter is the focus of this article. Yin et al. (2019a) discussed the relationship between early winter (December and January) haze days and the sea ice in the western part of the Beaufort Sea in September and October, the link

being the increased November SST in the Bering Sea and Gulf of Alaska. In Yin et al. (2019a) and herein, the areas of SST are quite different. As can be seen from Figs. 2 and 4, SST anomalies present a tripolar distribution. Our study focuses on regions of decreased SST, which have a considerable effect on the meteorological conditions in late winter over the NCP. In fact, from only the CC between HDI in late winter and Pacific SST, the SST in the Gulf of Alaska is also significantly correlated with the HDI. However, increased SST in the Gulf of Alaska is not enough to create suitable meteorological conditions for the haze to form in the NCP in late winter (Fig. S10). This is why our studies focus on only regions of decreased SST. When studying early-winter haze days, the increased SST region in triple pattern (Bering Sea and Gulf of Alaska) is the important connection between sea ice and haze days. The influences of SST in different regions of the Pacific Ocean on the meteorological conditions over the NCP are also different, and the complex mechanism of this difference requires in-depth research. This will be the focus of our next work.

We divide winter into two periods because there are considerably fewer haze days in late winter than in early winter. The trends of haze days in these two periods are also different, especially after the winter of 2013 (December in 2013 and January–March in 2014), with the numbers of haze days in early and late winter exhibiting opposite trends. Yin et al. (2019b) speculated that the Spring Festival in February was not the key reason

for February haze days reduced and that the climate anomalies may be the reasons. Through analysis, we found that haze pollution in the later winter was closely related to sea ice. As can be seen from Fig. 1(b), SI_SC decreased significantly from October 2013 to October 2016, and HDI also decreased significantly after February and March in 2014. This decrease in SI_SC may play a role in there being different trends for the numbers of haze days in late winter and early winter after 2013. The haze pollution in early winter in NCP was closely related to the Beaufort Sea ice in September and October and the snow cover in October and November in Eurasia (Yin et al. 2019a; Yin and Wang, 2018). The positive anomaly in Beaufort Sea ice and increased Eurasian snow cover increase the haze days in early winter. The external forcing factors affecting haze pollution in early and late winter are different, and their changes after 2013 are different, which may be the reason for the different trends for the numbers of haze days in late winter and early winter after 2013. However, convincing reasons and solid mechanisms for that difference remain unclear and require further research. Yin et al. (2019b) analyzed the relationship between Chukchi sea ice in early winter and February haze, the correlation decreased in recent years. Compared with that study, the anomaly signal of sea ice in this research appeared earlier, and due to different physical mechanisms, the correlation between sea ice anomaly in October and haze days in late winter is significant in recent years. The sea ice in October over East Siberian Sea and

Chukchi Sea is a good indicator of haze days in late winter.

References

Alexander MA, Bhatt US, Walsh JE, Timlin MS, Miller JS, Scott JD (2004) The Atmospheric Response to Realistic Arctic Sea Ice Anomalies in an AGCM during Winter. JOURNAL OF CLIMATE 17:890-905

Balmaseda MA, Ferranti L, Molteni F, Palmer TN (2010) Impact of 2007 and 2008 Arctic ice anomalies on the atmospheric circulation: Implications for long-range predictions. Quarterly Journal of the Royal Meteorological Society 136:1655-1664 doi:10.1002/qj.661

Cai W, Li K, Liao H, Wang H, Wu L (2017) Weather conditions conducive to Beijing severe haze more frequent under climate change. Nat Clim Change 7:257-262 doi:10.1038/Nclimate3249

Che H, Zhang X, Li Y, Zhou Z, Qu JJ, Hao X (2009) Haze trends over the capital cities of 31 provinces in China, 1981-2005. Theor Appl Climatol 97:235-242 doi:10.1007/s00704-008-0059-8

Chen H, Wang H (2015) Haze Days in North China and the associated atmospheric circulations based on daily visibility data from 1960 to 2012. journal of Geophysical Research: Atmospheres 120:5895-5909 doi:10.1002/2015JD023225

Chen H, Wang H, Sun J, Xu Y, Yin Z (2019a) Anthropogenic fine particulate matter pollution will be exacerbated in eastern China due to 21st century GHG warming. Atmos. Chem. Phys. 19: 233-243 doi:10.5194/acp-19-233-2019

Chen S, Guo J, Song L, Li J, Liu L, Cohen JB (2019b) Inter-annual variation of the spring haze pollution over the North China Plain: Roles of atmospheric circulation and sea surface temperature. International Journal of Climatology 39: 783-798 doi: 10.1002/joc.5842

Deser C, Tomas RA, Peng S (2007) The transient atmospheric circulation response to north atlantic sst and sea ice anomalies. J. Climate 20: 4751-4767 doi: 10.1175/JCLI4278.1

Deser C, Teng H (2008) Evolution of arctic sea ice concentration trends and the role of atmospheric circulation forcing, 1979–2007. Geophysical Research Letters 35(2): L02504 doi: 10.1029/2007GL032023

Ding Y, Liu Y (2014) Analysis of long-term variations of fog and haze in China in recent 50 years and their relations with atmospheric humidity. Science China Earth Sciences 57:36-46 doi:10.1007/s11430-013-4792-1

Gao H, Li X (2015) Influences of El Nino Southern Oscillation events on haze frequency in eastern China during boreal winters. International Journal of Climatology 35:2682-2688 doi:10.1002/joc.4133

Jacob DJ, Winnerb DA (2009) Effect of climate change on air quality. Atmospheric Environment 43:51-63 doi:10.1016/j.atmosenv.2008.09.051

Jia B, Wang Y, Huang S, Nan Y, Zhou X (2018) Variations of Siberian High Position under climate change: Impacts on winter pollution over north China. Atmospheric Environment 189:227-234 doi:10.1016/j.atmosenv.2018.06.045

Kay JE et al. (2015) The Community Earth System Model (CESM) Large Ensemble Project: A community resource for studying climate change in the presence of internal climate variability. BAMS 96:1333-1349 doi:10.1175/BAMS-D-13-00255.1

Kunii O, Kanagawa S, Yajima I, Hisamatsu Y, Yamamura S, Amagai T, Ismail ITS (2002) The 1997 haze disaster in Indonesia: Its air quality and health effects. Arch Environ Health 57:16-22 doi:Doi 10.1080/00039890209602912

Li F, Wang H (2013) Relationship between Bering Sea ice cover and East Asian winter monsoon year-to-year variations. Advances in Atmospheric Sciences 30:48-56 doi:10.1007/s00376-012-2071-2

Li F, Wang H (2014) Autumn Eurasian snow depth, autumn Arctic sea ice cover and East Asian winter monsoon. International Journal of Climatology 34:3616-3625 doi:10.1002/joc.3936

Li H, Chen H, Wang H (2017) Influence of North Pacific SST on heavy precipitation events in autumn

over North China. Atmospheric and Oceanic Science Letters 10:21-28 doi:10.1080/16742834.2017.1237256

Li Q, Zhang R, Wang Y (2016) Interannual variation of the wintertime fog-haze days across central and eastern China and its relation with East Asian winter monsoon. International Journal of Climatology 36:346-354

Li S, Lu J, Huang G, Hu K (2008) Tropical Indian Ocean Basin Warming and East Asian Summer Monsoon: A Multiple AGCM Study. Journal of Climate 21:6080-6088 doi:10.1175/2008JCLI2433.1

Lin Z, Li F (2018) Impact of interannual variations of spring sea ice in the Barents Sea on East Asian rainfall in June. Atmospheric and Oceanic Science Letters 11 doi:10.1080/16742834.2018.1454249

Liu J, Curry JA, Wang H, Song M, Horton RM (2012) Impact of declining Arctic sea ice on winter snowfall. Proceedings of the National Academy of Sciences of the United States of America 109:4074-4079 doi:10.1073/pnas.1114910109

Mori M, Watanabe M, Shiogama H, Inoue J, Kimoto M (2014) Robust Arctic sea-ice influence on the frequent Eurasian cold winters in past decades. Nature Geoscience 7:869 doi:10.1038/ngeo2277

Mu M, Zhang R (2014) Addressing the issue of fog and haze: A promising perspective from meteorological science and technology. SCIENCE CHINA Earth Sciences 57:1-2 doi:10.1007/s11430-013-4791-2

Neale R B and coauthors (2010) Description of the NCAR Community Atmosphere Model (CAM 4.0), Technical Report NCAR/TN-485+STR, National Center for Atmospheric Research, 7 pp., 2010.

Niu F, Li Z, Li C, Lee K-H, Wang M (2010) Increase of wintertime fog in China: Potential impacts of weakening of the Eastern Asian monsoon circulation and increasing aerosol loading. Journal of Geophysical Research: Atmospheres 115:D00K20 doi:10.1029/2009jd013484

Quan J, Zhang Q, He H, Liu J, Huang M, Jin H (2011) Analysis of the formation of fog and haze in North China Plain (NCP). Atmos Chem Phys 11:8205-8214 doi:10.5194/acp-11-8205-2011

Rayner NA, Parker DE, Horton EB, Folland CK, Alexander LV, Rowell DP, Kent EC, Kaplan A (2003) Global analyses of sea surface temperature, sea ice, and night marine air temperature since the late nineteenth century. J. Geophys. Res. 108(D14)4407 doi:10.1029/2002JD002670

Sun B (2017) Seasonal evolution of the dominant modes of the Eurasian snowpack and atmospheric circulation from autumn to the subsequent spring and the associated surface heat budget. Atmospheric and Oceanic Science Letters 10:191-197 doi:10.1080/16742834.2017.1286226

Wang H (2018) On assessing haze attribution and control measures in China. Atmospheric and Oceanic Science Letters 11:120-122 doi:10.1080/16742834.2018.1409067

Wang H, Chen H (2016) Understanding the recent trend of haze pollution in eastern China: roles of climate change. Atmos Chem Phys 16:4205-4211 doi:10.5194/acp-16-4205-2016

Wang H, Chen H, Liu J (2015) Arctic Sea Ice Decline Intensified Haze Pollution in Eastern China. Atmospheric and Oceanic Science Letters 8:1-9 doi:10.3878/aosl20140081

Wang J, Zhu Z, Qi L, Zhao Q, He J, Wang XLJ (2019) Two pathways of how remote SST anomalies drive the interannual variability of autumnal haze days in the Beijing–Tianjin–Hebei region, China. Atmos Chem Phys 19:1521-1535 doi: 10.5194/acp-19-1521-2019

Wang L, Zhang N, Liu Z, Sun Y, Ji D, Wang Y (2014a) The Influence of Climate Factors, Meteorological Conditions, and Boundary-Layer Structure on Severe Haze Pollution in the Beijing-Tianjin-Hebei Region during January 2013. Adv Meteorol 2014:ID 685971 doi:Artn 68597110.1155/2014/685971

Wang S, Liu J (2016) Delving into the relationship between autumn Arctic sea ice and central eastern Eurasian winter climate. Atmospheric and Oceanic Science Letters 9:366-374 doi:10.1080/16742834.2016.1207482

Wang Y, Yao L, Liu Z, Ji D, Wang L, Zhang J (2013) Formation of haze pollution in Beijing–Tianjin–Hebei region and their control strategies (in Chinese). *Bull. Chinese Acad. Sci.*, **28**, 353–363, 2013.

Wang Z et al. (2014b) Modeling study of regional severe hazes over mid-eastern China in January 2013 and its implications on pollution prevention and control. Sci China Earth Sci 57:3-13 doi:10.1007/s11430-013-4793-0

Xiao D, Li Y, Fan S, Zhang R, Sun J, Wang Y (2015) Plausible influence of Atlantic Ocean SST anomalies on winter haze in China. Theoretical and Applied Climatology 122:249-257 doi:10.1007/s00704-014-1297-6

Xu X, He S, Li F, Wang H (2018) Impact of northern Eurasian snow cover in autumn on the warm Arctic–cold Eurasia pattern during the following January and its linkage to stationary planetary waves. Climate Dynamics 50:1993-2006 doi:10.1007/s00382-017-3732-8

Yang Y, Liao H, Lou S (2016) Increase in winter haze over eastern China in recent decades: Roles of variations in meteorological parameters and anthropogenic emissions. Journal of Geophysical Research: Atmospheres 121:13050-03065 doi:10.1002/2016JD025136

Yin Z, Wang H, Guo W (2015) Climatic change features of fog and haze in winter over North China and Huang-Huai Area. Science China: Earth Sciences 58: 1370–1376 doi: 10.1007/s11430-015-5089-3

Yin Z, Wang H (2016) The relationship between the subtropical Western Pacific SST and haze over North-Central North China Plain. International Journal of Climatology 36:3479-3491 doi:10.1002/joc.4570

Yin Z, Wang H (2017a) Role of atmospheric circulations in haze pollution in December 2016. Atmos Chem Phys 17:11673-11681 doi:10.5194/acp-17-11673-2017

Yin Z, Wang H (2017b) Statistical Prediction of Winter Haze Days in the North China Plain Using the Generalized Additive Model. Journal of Applied Meteorology and Climatology 56:2411-2419 doi:10.1175/jamc-d-17-0013.1

Yin Z, Wang H (2018) The strengthening relationship between Eurasian snow cover and December haze days in central North China after the mid-1990s. Atmos Chem Phys 18:4753-4763

doi:10.5194/acp-18-4753-2018

Yin Z, Wang H, Chen H (2017) Understanding severe winter haze events in the North China Plain in 2014: roles of climate anomalies. Atmos Chem Phys 17:1641-1651 doi:10.5194/acp-17-1641-2017

Yin Z, Li Y, Wang H (2019a) Response of early winter haze days in the North China Plain to Autumn Beaufort Sea ice, Atmos Chem Phys 19: 1439-1453 doi:10.5194/acp-19-1439-2019

Yin Z, Wang H, Ma X (2019b) Possible relationship between the Chukchi Sea Ice in the Early Winter and the February haze pollution in the north China plain, J. Climate 32: 5179-5190 doi:10.1175/JCLI-D-18-0643.1

Yin Z, Wang H, Li Y, Ma X, Zhang X (2019c) Links of Climate Variability among Arctic sea ice, Eurasia teleconnection pattern and summer surface ozone pollution in North China, Atmos. Chem. Phys., 19: 3857-3871 doi:10.5194/acp-19-3857-2019

Zhang R, Li Q, Zhang R (2014) Meteorological conditions for the persistent severe fog and haze event over eastern China in January 2013. Sci China Earth Sci 57:26-35 doi:10.1007/s11430-013-4774-3

Zhang X, Wang Y, Niu T, Zhang X, Gong S, Zhang Y, Sun J (2012) Atmospheric aerosol compositions in China: spatial/temporal variability, chemical signature, regional haze distribution and comparisons with global aerosols. Atmos Chem Phys 12:779-799 doi:10.5194/acp-12-779-2012

Zhang Y et al. (2016) Impact of synoptic weather patterns and inter-decadal climate variability on air quality in the North China Plain during 1980–2013. Atmospheric Environment 124:119-128

Zhong W, Yin Z, Wang H (2019) The relationship between the anticyclonic anomalies in Northeast Asia

and severe haze in the Beijing–Tianjin–Hebei region. Atmos. Chem. Phys. 19: 5941-5957

doi:10.5194/acp-19-5941-2019

Zuo J, Ren H, Wu B, Li W (2016) Predictability of winter temperature in China from previous autumn

Arctic sea ice. Climate Dynamics 47:2331-2343 doi:10.1007/s00382-015-2966-6

(a) SI│HDI

(b)
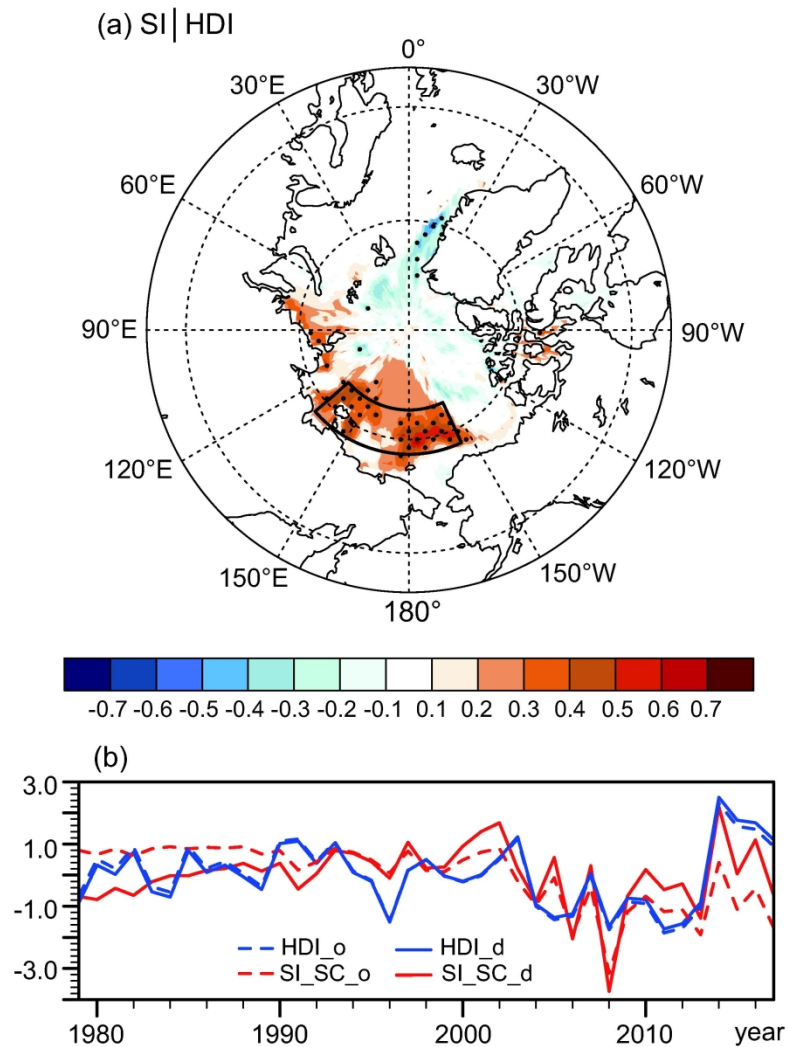
Quan Yang, Fig. 1 (a) Correlation coefficient (CC) between haze-day index (HDI) in late winter and Arctic sea-ice concentration (SIC) in October from 1978 to 2016. The black box area is the selected East Siberian Sea and Chukchi Sea. The black dots indicate where the CC exceeded the 95% confidence level. (b) Standardized interannual variations in HDI and sea-ice index over the East Siberian Sea and Chukchi Sea (SI_SC) before de-trending (dashed lines) and after de-trending (solid lines).
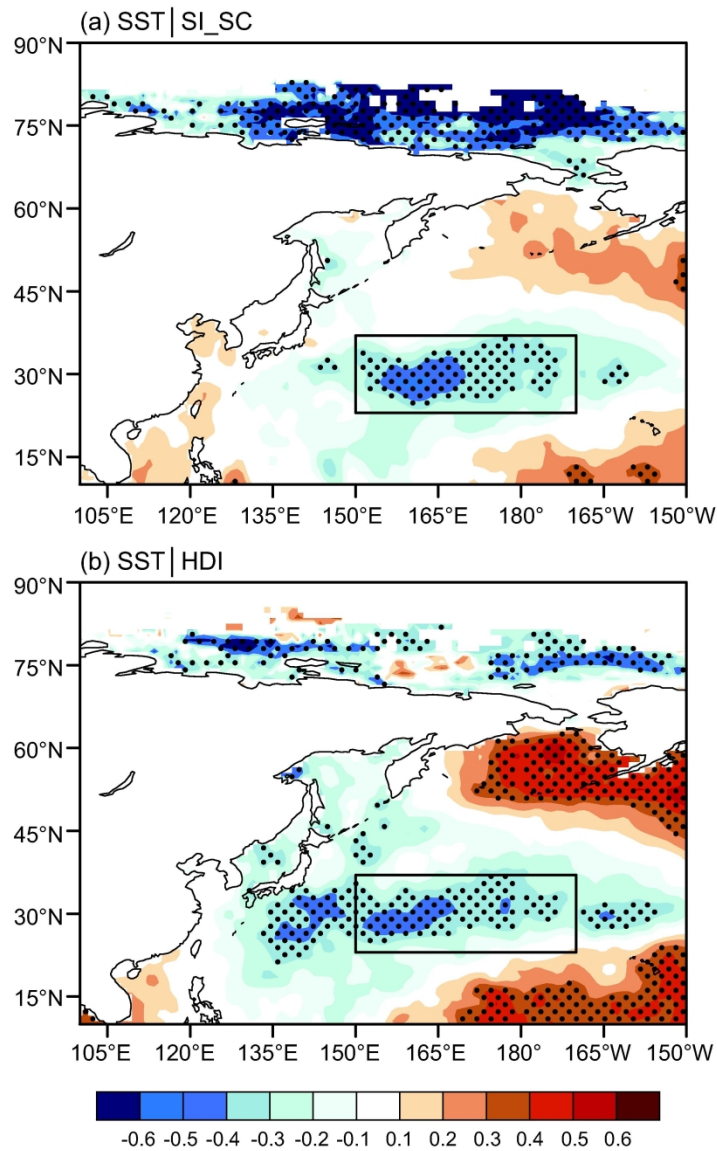
Quan Yang, Fig. 2 CC between sea surface temperature (SST) in October and November and (a) SI_SC in October, (b) HDI in late winter. The black dots indicate where the CC exceeded the 95% confidence level. The rectangular area is the selected Minami-Tori Shima and Midway Atoll region in October and November.
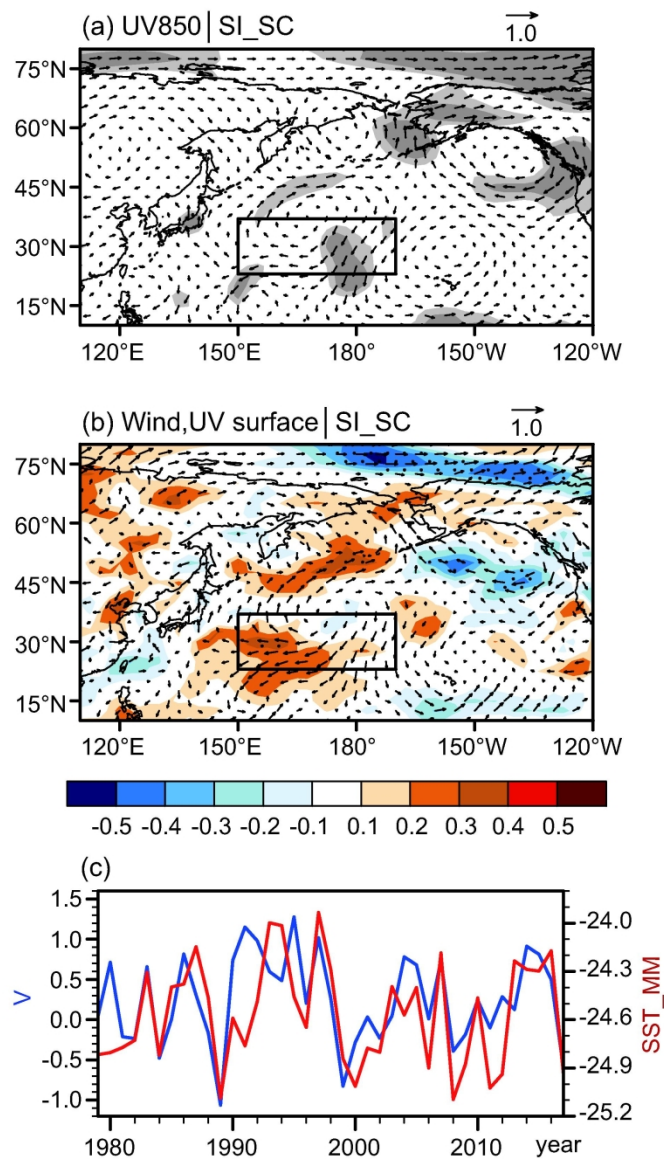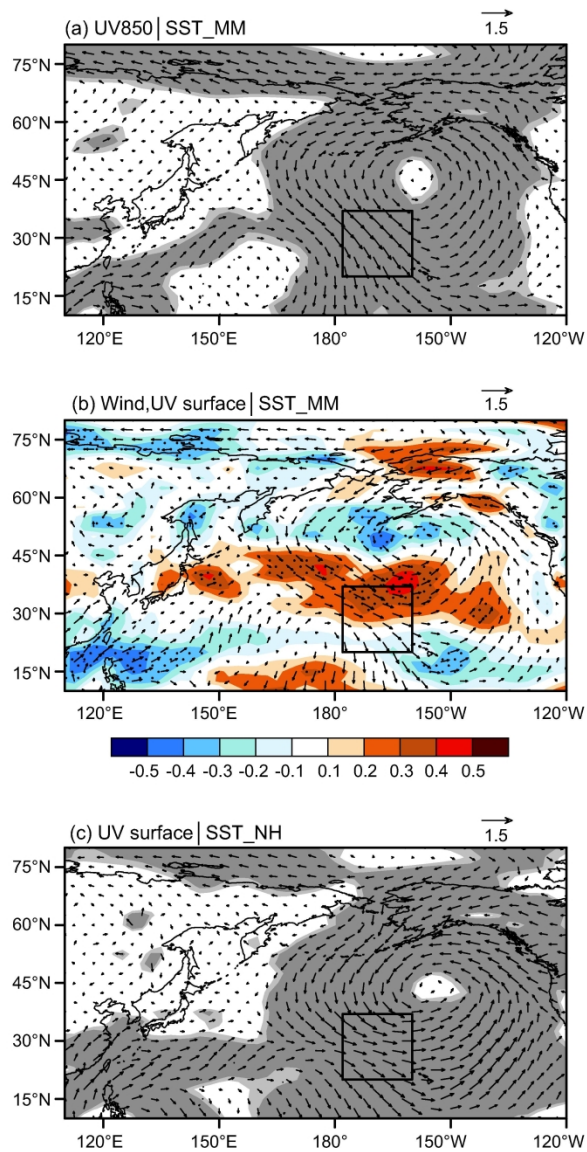
Quan Yang, Fig. 3 (a) CC between SI_SC and wind vector at 850 hPa in October and November. The light and dark shading indicate where the CC exceeded the 90% and 95% confidence levels, respectively. (b) CC between SI_SC and wind vector at surface (arrows), surface wind speed (shading) in October and November. The black dots indicate where the CC exceeded the 95% confidence level. (c) Variation in meridional wind index (blue) and SST index over Minami-Tori Shima and Midway Atoll (SST_MM, red) in October and November. The rectangular area in (a) and (b) is the selected Minami-Tori Shima and Midway Atoll region in October and November.
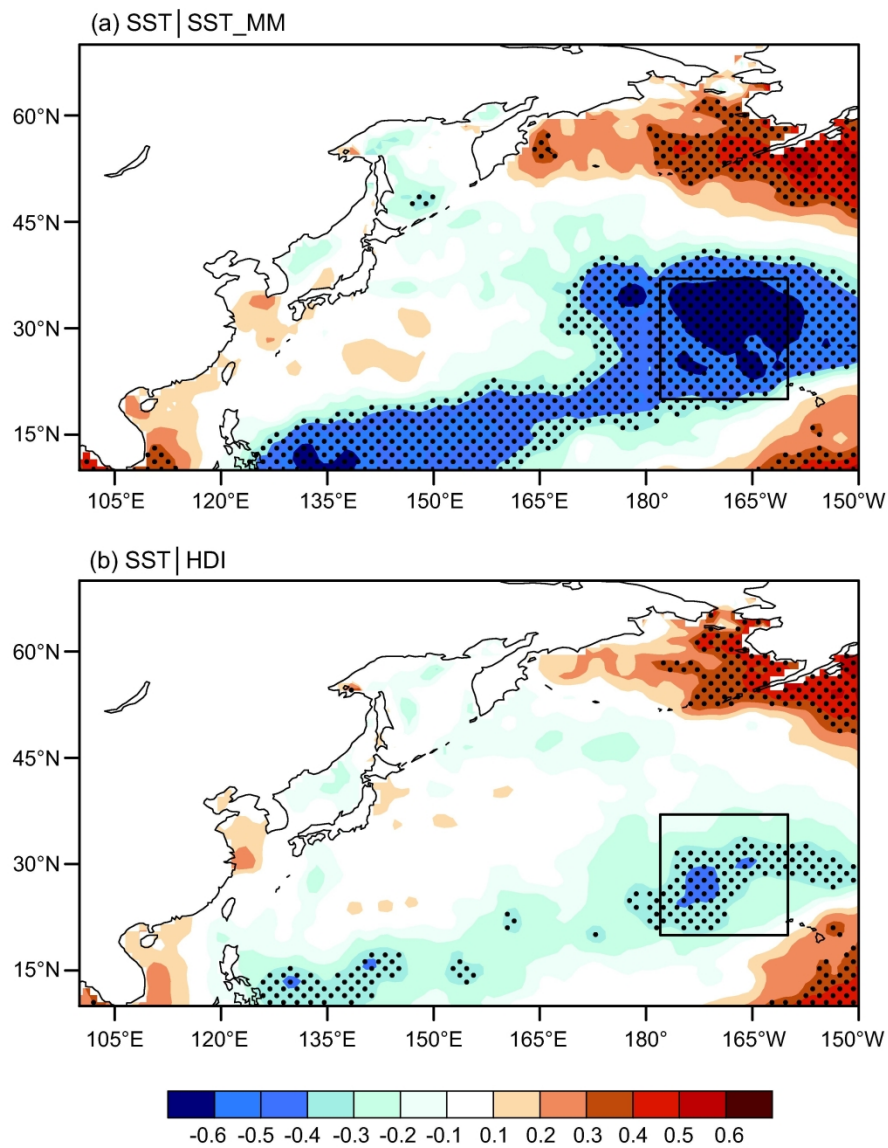
Quan Yang, Fig. 4 CC between SST in January and February and (a) SST_MM, (b) HDI in late winter. The black dots indicate where the CC exceeded the 95% confidence level. The rectangular area is the selected northwest of the Hawaiian Islands region in January and February.
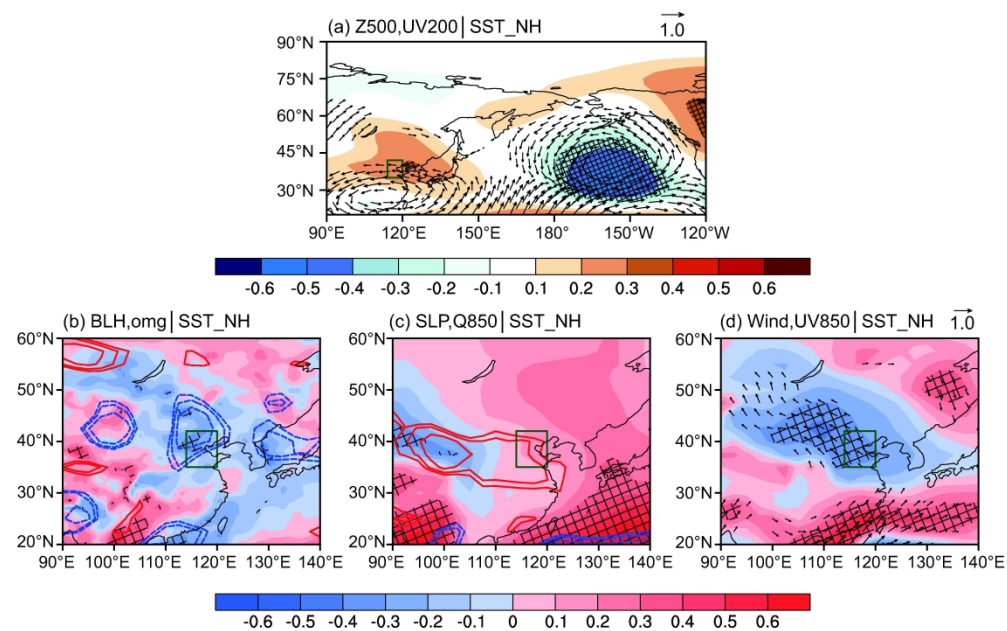
Quan Yang, Fig. 5 (a) CC between SST_MM and wind vector at 850 hPa in January and February. (b) CC between SST_MM and wind vector at surface (arrows), surface wind speed (shading) in January and February. The black dots indicate where the CC exceeded the 95% confidence level. (c) CC between SST index of the northwestern side of the Hawaiian Islands (SST_NH) and wind vector at surface in January and February. The light and dark shading in (a) and (c) indicate where the CC exceeded the 90% and 95% confidence levels, respectively. The rectangular area is the selected northwest of the Hawaiian Islands region in January and February.
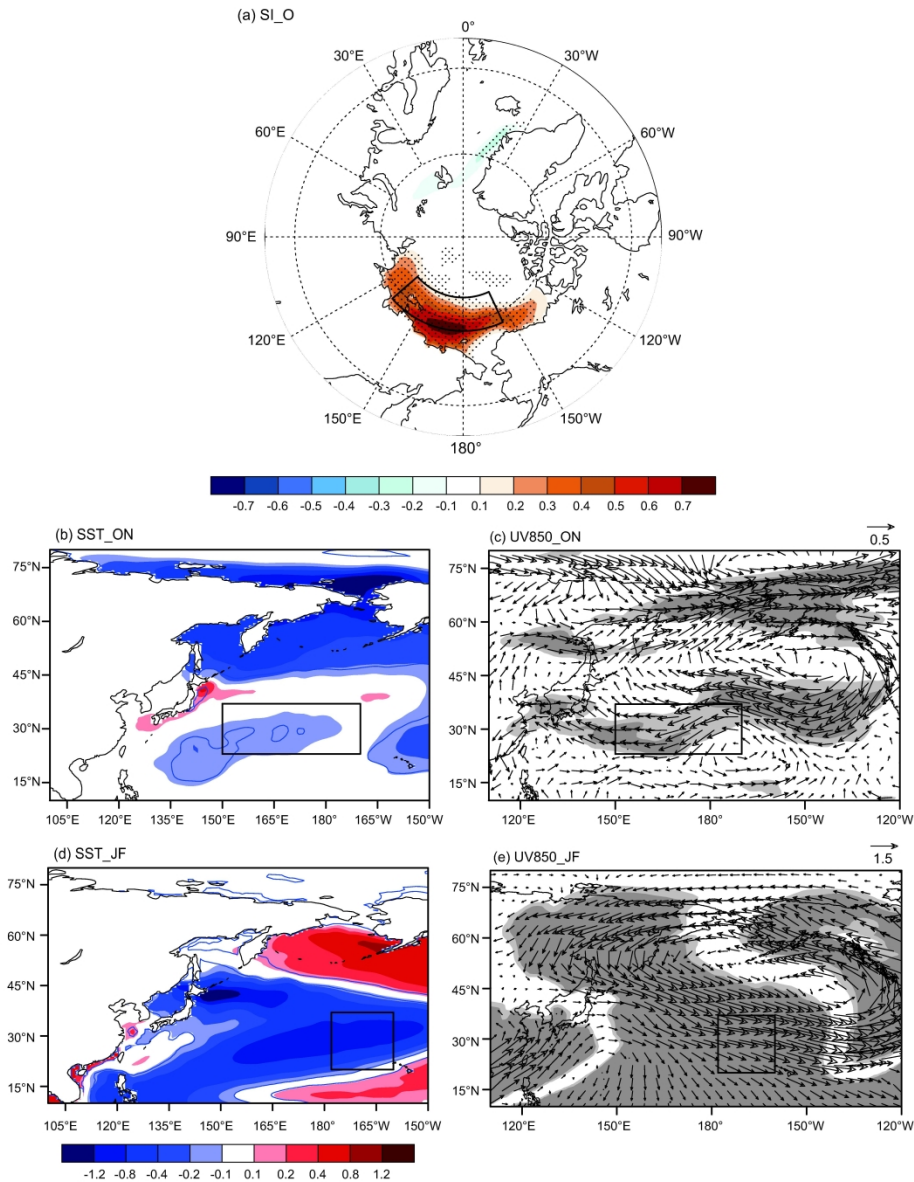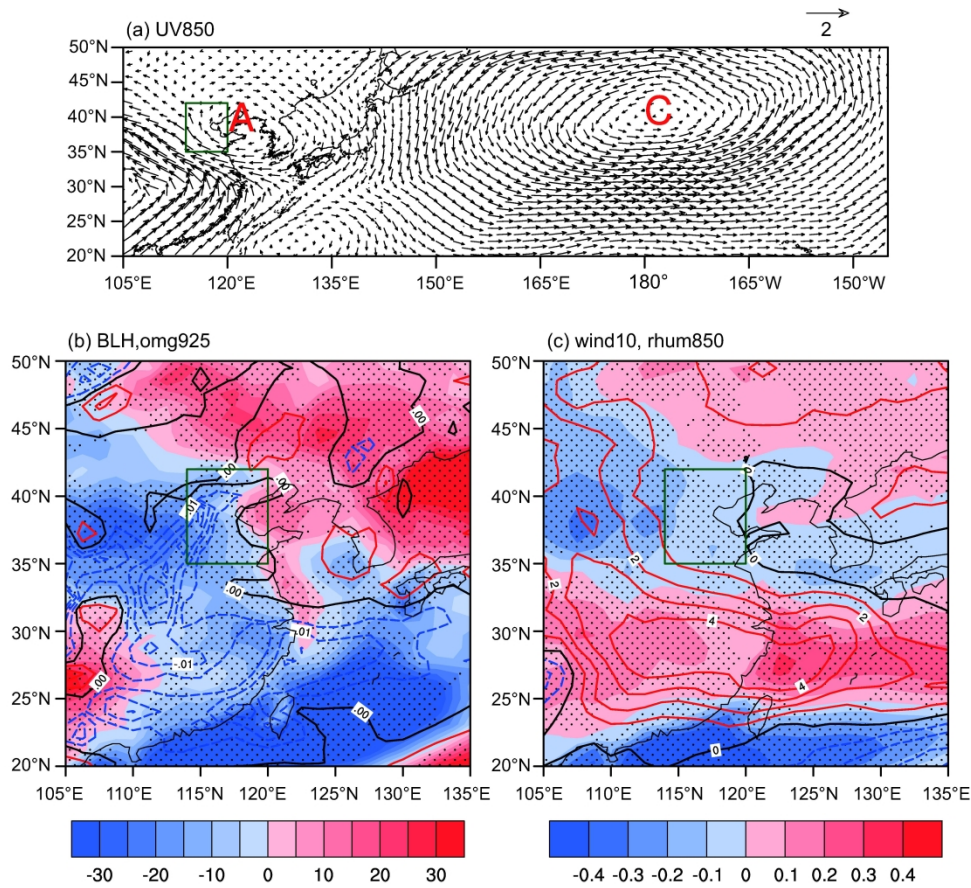
Quan Yang, Fig. 6 Composite differences based on Community Earth System Model Large Ensemble (CESM_LE) of (a) Arctic SIC in October, (b) (d) SST, (c) (e) wind vector at 850 hPa in (b) (c) October and November from 1978 to 2016 and (d) (e) January and February from 1979 to 2017. The blue contours in (b) and (d) indicate where the differences exceeded the 95% confidence level. The light and dark shading in (c) and (e) indicate where the differences exceeded the 90% and 95% confidence levels, respectively. The rectangular areas are the selected Pacific Ocean regions.

Quan Yang, Fig. 7 CC between SST_NH and (a) Z500 (shading) and wind at 200 hPa (arrows), (b) boundary-layer height (BLH) (shading) and surface omega (contours), (c) sea-level pressure (SLP) (shading) and specific humidity at 850 hPa (contours), (d) wind vector (arrow) and wind speed (shading) at 850 hPa in late winter from 1979 to 2017. The black grids indicate where the CC exceeded the 95% confidence level, and the three contours indicate where the CC exceeded the 90%, 95%, and 99% confidence levels, respectively. The dark-green rectangular area is the NCP.

Quan Yang, Fig. 8 Composite differences of (a) wind vector at 850 hPa, (b) BLH (shading) and omega at 925 hPa (contours), (c) wind speed (shading) at 10 m and relative humidity at 850 hPa (contours) in late winter between two sensitivity experiments with version 4 of the Community Atmosphere Model (CAM4). The black dots indicate where changes from more than 50% of the 30 members in BLH and 10-m wind speed are consistent with the ensemble mean. The dark-green rectangular area is the NCP.
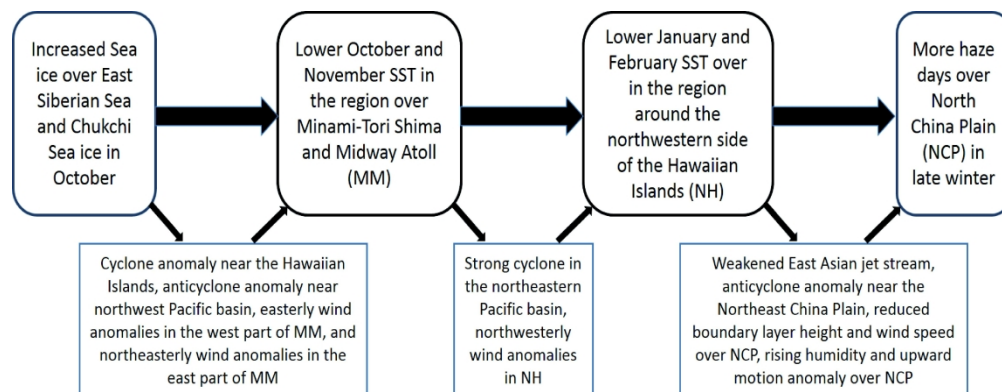
Quan Yang, Fig. 9 Schematic of mechanism whereby October SI_SC affects number of haze days in late winter over the North China Plain